Highly Miniaturized Octa-band Antenna Using Concentric Circular Split Ring Structures

Original Scientific Paper

Padmaja Priyadarsini P
School of Electronics Engineering
VIT-AP University
Amaravathi, Andhra Pradesh - 522237, India
priyadarsini.20phd7143@vitap.ac.in

Chandu DS *
School of Electronics Engineering
VIT-AP University
Amaravathi, Andhra Pradesh - 522237, India
chandu.ds@vitap.ac.in

*Corresponding author

Abstract *– The proposed antenna design represents a systematic evolution from a simple ring-shaped structure to a highly efficient and versatile multi-band configuration tailored for next-generation wireless communication systems. Through the integration of rectangular slots, circular-shaped split ring resonators (CSRRs), and optimized geometries, the antenna achieves octa-band operation with superior impedance matching, enhanced bandwidth, and improved performance over a wide frequency range. The antenna is designed to support communication bands, including 4G/3G/2G, Wi-Fi, WLAN, WiMAX, and sub-6 GHz 5G connectivity. It resonates at 1.22, 2.12, 3.00, 4.76, 5.40, 5.94, 6.70, and 7.44 GHz, with a compact electrical size of 0.08 λ0 × 0.08 λ0. The inclusion of CSRRs and slots significantly expands the operational frequency bands while achieving a radiation efficiency of 84% and a peak gain of 4.1 dBi, making it well-suited for modern wireless applications. Moreover, the antenna design simplifies manufacturing and reduces the costs. Its compact and efficient structure ensures seamless integration into portable devices such as tablets and laptops, addressing the challenges of system complexity, size, and cost. This antenna provides a practical and scalable solution to meet the demands of diverse frequency bands in modern communication systems.*

Keywords*:* *Antenna design, CSSRR Resonator, Octa band, Gain and radiation efficiency, HFSS*

Received: December 10, 2024; Received in revised form: April 8, 2025; Accepted: April 8, 2025

1. INTRODUCTION

Over the past two decades, the rapid evolution of modern wireless personal communication devices, such as smartphones, has driven the demand for antennas capable of operating across multiple frequency bands while maintaining omnidirectional radiation characteristics. The integration of various wireless standards [1], including Bluetooth, WLAN, IOT, 5G sub-6 GHz, Wi-MAX [2-4], and RFID, necessitates antennas that can support diverse frequency ranges within the spatial constraints of compact devices. This presents a significant challenge for antenna researchers in designing structures that balance miniaturization with performance.

To address these challenges, several antenna design techniques have been developed to support multi-band functionality. Multi-band antennas offer a distinct advantage by reducing system complexity and physical dimensions, as a single antenna can cater to multiple applications. Antenna design plays an important role in determining essential parameters such as bandwidth, radiation efficiency, and overall system performance.

Microstrip patch antennas have emerged as a preferred choice for most wireless applications due to their inherent advantages, including compact size, lightweight construction, low fabrication cost, planar structure, and the ability to operate across multiple frequency bands. These features make microstrip patch antennas suitable for integration into modern devices, eliminating the need for multiple antennas to accommodate different resonant frequencies [5-7]. Consequently, these antennas are extensively employed in contemporary wireless communication systems, aligning with the requirements of advanced technologies and applications.

Various topologies are used for enhancing multi-band antenna. These typologies require extra space in the system to accommodate the external multiplexer circuits needed to choose the frequency bands. Multiple bands can be used at once with the latest generation of antennas, which also have intrinsic multiplexing properties. Metamaterial structures commonly used include Split-Ring Resonators (SRRs) [8, 9] and Complementary Split-Ring Resonators (CSRRs) [10, 11]. SRRs typically consist of two split rings facing in opposite directions and can take on various shapes such as rings, circles, squares, triangles, and hexagons. The rings function as resonators because of the presence of inductors as well as capacitors in the metal ring, and the resonant frequency can be refined by altering aspects such as split gap, metal width, spacing between adjacent rings, adjacent length, as well as presenting multiple split gaps. Reference [6] showcases the design, fabrication, and testing of a hexa-band monopole antenna with a low profile. Applications for 3G Advanced, Wi-Fi, WLAN, and WiMAX are all within the scope of the intended planar monopole antenna. A microstrip patch antenna [10] is constructed and studied for six working bands with slight frequency ratios with slender RF channel frequencies. An innovative four inverted L-shaped slots on a patch antenna is suggested for use with hexa-band circular shapes presented in [14]. The suggested antenna, which has a small footprint and operates on the Hexa-band frequency, is well-suited for a variety of uses, including those involving RADAR, Bluetooth, 5G mid-band, WiMAX, WLAN, LTE, as well as Wi-Fi [15]. A miniaturized hexa- band monopole antenna with circular polarization is expected to have multiple uses in [16] it is possible that WLANs and other wireless communication equipment would benefit from the suggested antenna. Hexa-band, dual-polarization performance is demonstrated by the favored design [17] at frequencies of 3,46, 8.28, 12.26, 17.21, 23,40, and 26.01. The miniature hexagonal fractal antenna has excellent improvement, high directionality, and an omnidirectional radiation outline throughout the multi-resonant frequency for 5G, IoT, satellite, and radar applications. This design [18] features a hexa-band PBG stacked MSPA that resonates between 1 and 9 GHz. In [16], a hepta-band resonance antenna for fifth-generation (5G) technology is planned. It is modeled on a Taconic TLY-3 substrate and resonates at a variety of frequencies that have been defined, including 28.1 GHz, 36.7 GHz, 45.8 GHz, 55.2 GHz, 62.8 GHz, 72.3 GHz, and 82 GHz accordingly. Antennas detailed in references [19-26] may receive signals on eight different service bands: PCS, LTE700, GSM850, GSM900, UMTS, DCS, LTE2500, and LTE2300. However, they have not been able to receive signals on the Wi-Fi, WiMAX, WLAN, or 5G bands. A total of seven service bands DCS, PCS, GSM850, GSM900, UMTS, LTE2500, and LTE2300 are covered by the antennas mentioned in references [27-31]. However, the Wi-Fi, WLAN, WiMAX, and 5G bands are not among them. There are works that reported miniaturization [32, 33] but the antennas are not multi- band and the design is complex.

The study of existing literature reveals that wireless communication systems require compact antennas with excellent performance in terms of bandwidth, gain, and efficiency. This research primarily focuses on the design of compact antennas for multi-band wireless applications in modern technologies. Specifically, it explores the performance of a single antenna that supports multiple applications while maintaining a compact size and high performance.

Key Advantages of the proposed antenna:

- The proposed antenna features a compact design utilizing a circular-shaped split ring resonator (CSSRR) structure with a full ground plane.
- It achieves octa-band operation, making it suitable for modern wireless communication applications.
- The design demonstrates a peak gain of 4.71 dBi and maintains a VSWR below 2 across all operating bands.
- Radiation efficiency ranges from 77% to 85% over the entire operating frequency range.
- The antenna is well-suited for defense tracking and weather monitoring applications due to its unique features.
- It is excited using a 50-ohm impedance-matched transmission line with full ground as reflector.
- The compact dimensions are 20 mm × 20 mm, with an electrical size of 0.08 $\lambda0 \times$ 0.08 $\lambda0$ at the lowest resonant frequency.
- The ground plane length is optimized to enhance performance across the bands.

To address these challenges, this work integrates modified circular ring structures, optimized slot placements, and multiple CSSRR configurations. The proposed antenna demonstrates superior multi-band performance, improved impedance matching, and enhanced radiation characteristics. Future enhancements could involve further optimization of the CSSRR configurations and the integration of meta- surfaces to achieve broader bandwidths and increased efficiency in practical applications.

2. ANTENNA DESIGN EVOLUTION

Fig. 1 illustrates the step-by-step evolution of the proposed design, labeled as Antenna 1, Antenna 2, Antenna 3, and Antenna 4. Table I provides the detailed measurements and parameter values for each stage. Initially, the ring-shaped antenna design has an outer radius R_1=9.3 mm, an inner radius R_2=6.8 mm, and a width w_1=2.5 mm. The ring-shaped antenna integrated a rectangular patch at its bottom, measuring y=1.95 mm in length and x=0.75 mm in width. The overall antenna includes a full ground plane measuring 20×20 mm^2.

This configuration achieved a resonant band at 3.16 GHz, as calculated using Equation 1. The simulated results were validated against the theoretical circular patch Equation 1, and the design is labeled as Antenna 1 in Fig. 1.

Further, the rectangular slot has been etched from Antenna 1 to develop a multi-band antenna. Fig. 1 labels the slot as Antenna 2, with a width (Rwx) of 0.5 mm. The antenna forms this slot in the traditional CSSRR shape. The inclusion of this slot resulted in the formation of a penta-band with resonant frequencies at 1.54 GHz, 3.18 GHz, 4.46 GHz, 6.24 GHz, and 7.46 GHz. Among these, only the resonant frequency at 6.24 GHz exhibits excellent impedance matching, while the reflection coefficients of the remaining four frequencies indicate poor impedance matching.

Table 1. Antenna Dimensions with detail Parameters

Parameter	R_1	R_2	R_3	R_w	R_{wx}
Dimension (mm)	9.3	6.8	5.8	1.85	0.5
Parameter	W_1	X	Y	W_2	G
Dimension (mm)	2.5	0.75	1.95	1.5	0.7
Parameter	X_1	R_4	R_5	-	-
Dimension (mm)	1.5	3.6	0.5	-	-

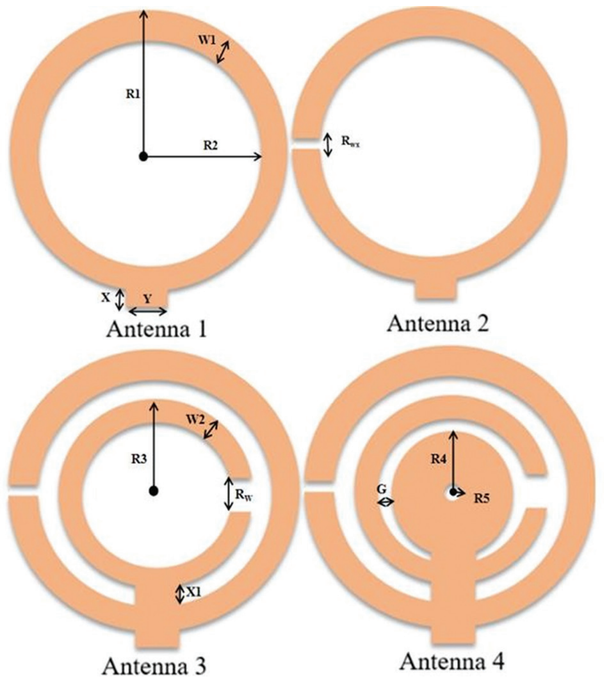

Fig. 1. The Evolution of the Proposed Antenna 1,2,3 and 4

In Antenna 3, a circular-shaped split ring resonator (CSSRR) with a radius (R_3) of 5.8 mm and a ring width (W_2) of 1.5 mm has been incorporated from Antenna 2. A rectangular slot with a length (y) of 1.85 mm and a width (x_1) of 1.5 mm has been connected to the first CSSRR. Additionally, a 1.85 mm-wide slot is etched from the second ring-shaped antenna to form the second CSSRR. This configuration resulted in a hexa-band antenna with resonant frequencies at 1.26 GHz, 2.22 GHz, 3.24 GHz, 4.06 GHz, 5.66 GHz, and 6.84 GHz. However, the lowest and highest frequencies exhibit poor impedance matching.

The circular-shaped antenna has a radius (R_4) of 3.6 mm, with a gap (G) of 0.7 mm for the second CSSRR. Additionally, a smaller radius (R_5) of 0.5 mm has been etched from the center of the main radiating element of R_4. This structure represents an optimized multi-band antenna with an improved performance. Through the integration of modified circular rings, CSRRs, and slots, the antenna achieves octa-band operation. The lowest frequency now exhibits better impedance matching compared to Antenna 3. The optimized antenna is shown in Fig. 1, labeled as Antenna 4.

The radiator of the antenna is composed of two circular-shaped split ring resonator elements of structure with different dimensions on a single-layer square-shaped FR4 substrate Generally, the approximate original value for the radius of the circular-shaped split ring with a radius of R1; thus, the exact value of R1 can be evaluated with the assistance of the consecutive circle patch radius Equitation 1.

$$a = \frac{F}{\left\{1 + \frac{2h}{\pi \in_r F}\left[ln\left(\frac{\pi F}{2h} + 1.7726\right)\right]\right\}^{0.5}} \qquad (1)$$

where $F = \frac{8.791 \times 10^9}{f_r \sqrt{\in_r}}$

Where 'a' is equal to the circular patch radius R_1. The following section presents the parametric study of the proposed antenna resonated at frequencies of 1.2, 2.1, 2.9, 4.7, 5.4, 5.9, 6.6, and 7.3 GHz.

Equivalent circuit is designed to further understand the evolution of the antenna. The circular shaped antenna shown in Fig. 2(a) can be represented as a series LC circuit. However, due to the center hole and the conductive nature of the circular patch, an additional resistance is added and the antenna is modeled using RLC circuit [34]. When the radius of the circular hole is increased, the antenna forms a split-ring structure and the equivalent parallel LC circuit defines the antenna (this is most commonly seen in the existing literature). The novelty of the paper is the multi-band response using a compact antenna design and when multiple split-rings are introduced in a concentric manner, the equivalent circuit is a series combination of LC circuits along with the initial RLC circuit as shown in Fig. 2(c). The capacitors (CR1, CR2, CR3) are the shunt capacitors, while CC1, CC2 and CC3 are the coupling capacitors that exist due to the coupling between the adjacent rings. Between the CR capacitor and the CC capacitor, there exists a coupling inductance LC. Fig. 2(d) shows the frequency response of the equivalent circuit model of the proposed antenna. Due to the coupling capacitors and LC resonant circuits an octa band response is achieved. The circuit simulation results match well with the full-wave simulation results with $<$ 5% deviation. The resonant frequencies achieved from the full-wave simulator are 1.2 GHz, 2.1 GHz, 2.9 GHz, 4.7 GHz, 5.4 GHz, 5.9 GHz, 6.6 GHz, and 7.3 GHz. The resonant frequencies obtained from the circuit- simulation are 1.24 GHz, 2.11 GHz, 2.9 GHz, 4.82 GHz, 5.48 GHz, 6.0 GHz, 6.72 GHz, and 7.32 GHz. Minor discrepancies can be attributed to the ideal circuit elements and material losses that are not considered in the circuit simulation.

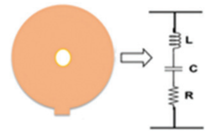

(a)

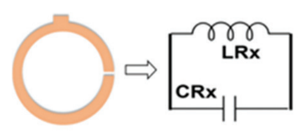

(b)

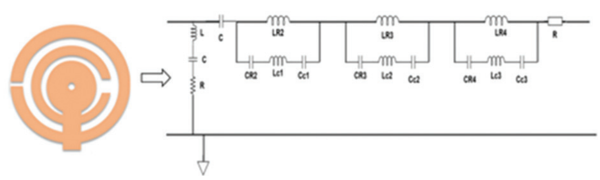

(c)

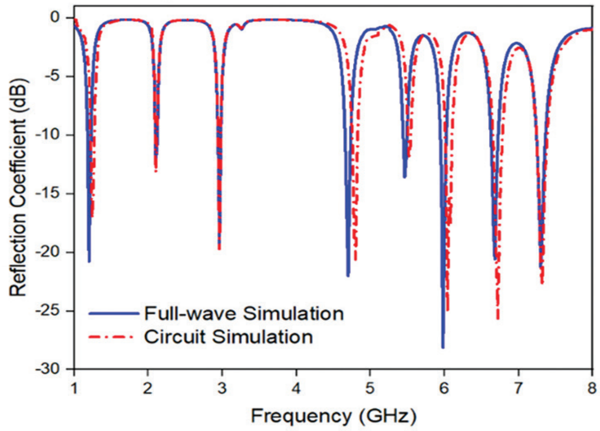

(d)

Fig. 2. The equivalent circuit of: (**a**) Circular-shaped antenna (**b**) CSSRR-shaped antenna, (**c**) Proposed model and (**d**) Comparison of the reflection coefficient of the proposed antenna with equivalent circuit response and full-wave simulation

3. PARAMETRIC ANALYSIS AND WORKING MECHANISM

The octa-band antenna's structure and each band's principle have been analyzed. The antenna has been simulated using commercial EM solver to examine the impact of various settings on matching, frequency shift, bandwidth, and gain. Fig. 3 and Fig. 4 depicts the impact of parameter adjustments on the reflection coefficient. Fig. 3(a) displays S_{11} with the effect of varying R_1 from 9.1 mm to 9.4 mm. The desired frequency with good return loss is attained only when $R_1 = 9.3$ mm . In the other cases, i.e., R_1 =9.1 mm, 9.2 mm, and 9.4 mm, the Octa-band response is not detected. The parametric analysis of the R_w parameter, as shown in Fig. 3(b), illustrates a variation from 1.65 mm to 1.95 mm. Based on the observation of the S11 results, the optimized R_w value is determined to be 1.85 mm. In the other cases i.e. at 1.65 mm, 1.75 mm, and 1.95 mm a frequency shift and impedance mismatch are observed. Fig. 4(a) shows the simulated S_{11} results by increasing the radius R_3 from 5.6 mm to 5.9 mm. The necessary band resonance occurs only when optimized R_3=5.8 mm, while other values result in a frequency shift in the higher bands. The Fig. 4(b) with S_{11} represents the influence of R_{wx} from 0.4 mm to 0.7 mm on the major radiating patch. Due to this, there is a minor difference in the upper three bands. This analysis tries to determine the suitable value of R_{wx} to get the accurate octa band.

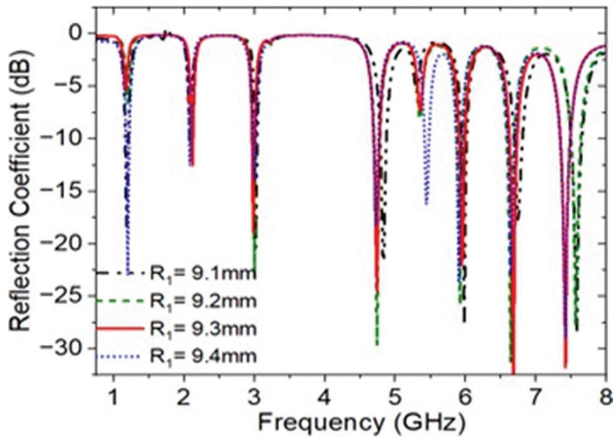

(a)

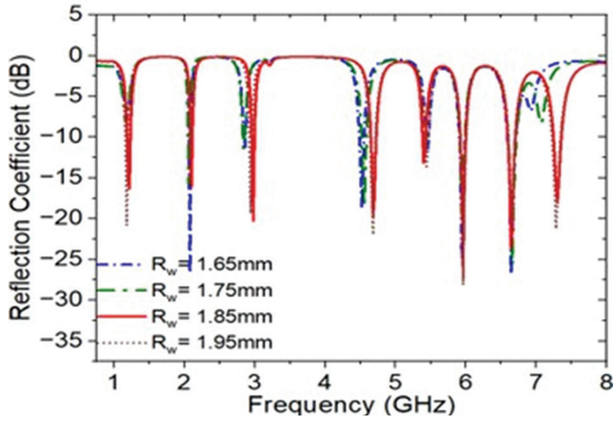

(b)

Fig. 3. Parametric analysis showing (**a**) Variation in R_1 (**b**) Variation in R_w

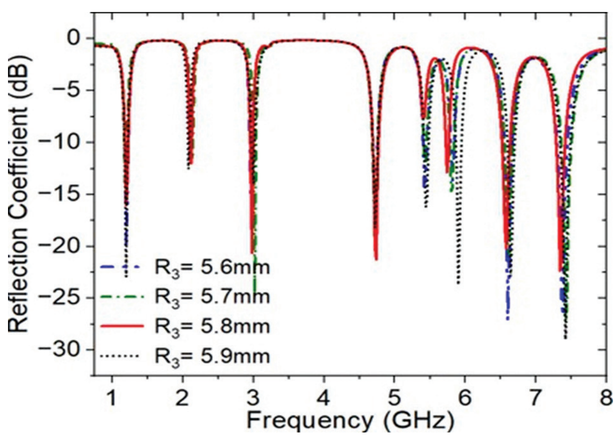

(a)

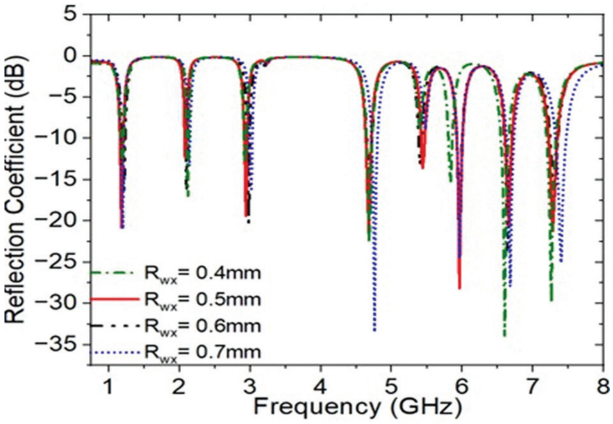

(b)

Fig. 4. Parametric analysis showing (**a**) Variation in R_3, (**b**) Variation in R_{wx}

Fig. 5 illustrates the surface current distribution at eight operational frequencies, revealing distinct patterns across the various frequencies.

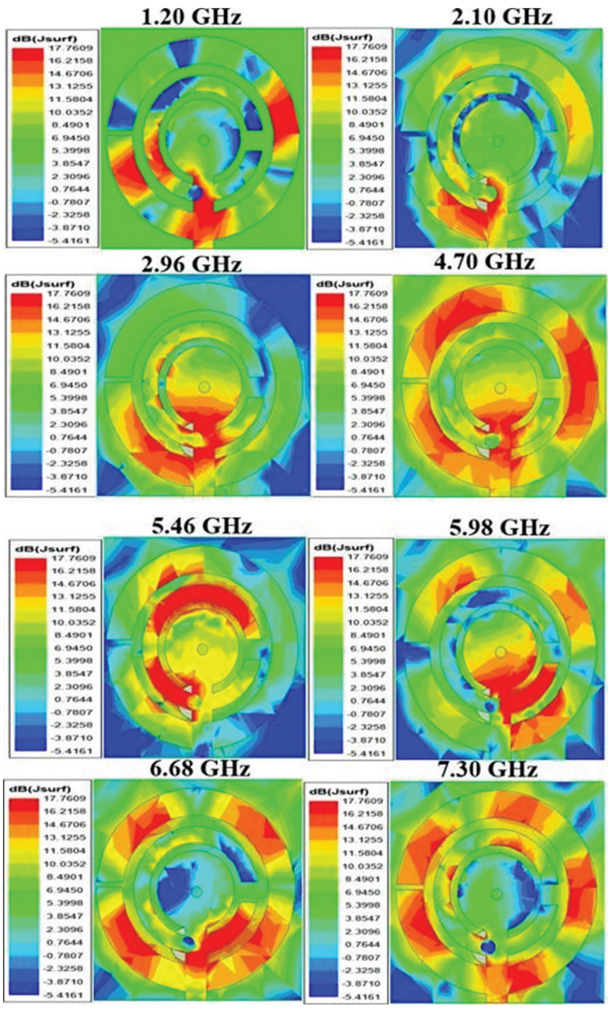

Fig.5. Surface current distribution of the resonating frequencies of the CSSRR antenna

At 1.20 GHz, the current is strong in the outer split-ring radiating area but weak in the central radiating area. At 2.10 GHz, the current is concentrated in the first and second split rings, with a small amount extending to the center. At 2.96 GHz, the current is intense around the feeding area and the right- side radiating area, while it is moderate on the opposite side. At 4.70 GHz and 6.68 GHz, the surface current is moderate in the central area and strong in the outer split- ring resonator. At 5.44 GHz, the current is strong in the inward split-ring resonator and weak in the outward split- ring resonator. At 5.84 GHz, the current is highly concentrated around the feeding position on the right side. Finally, at 6.68 GHz and 7.30 GHz, the surface current distribution is strong in the outer ring. These observations provide valuable insights into the antenna's behavior at different operational frequencies.

4. RESULTS AND DISCUSSION

To assess the effectiveness of the designed antenna, a prototype was fabricated and Fig. 6 presents the optimized antenna design with dimensions, including both the front and rear views, alongside the fabricated model.

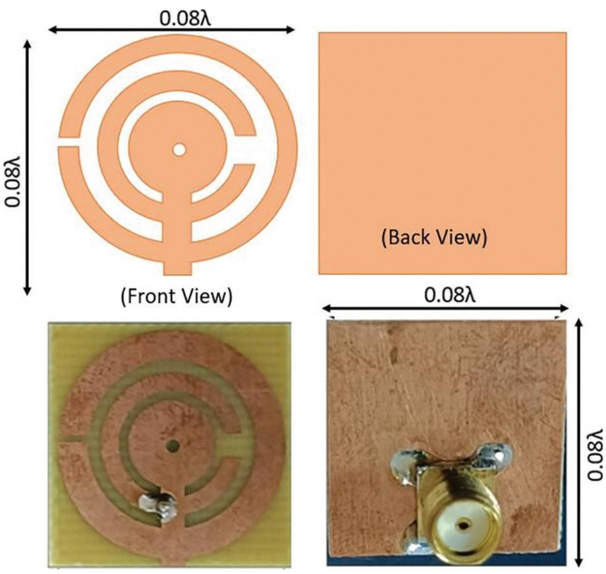

Fig. 6. Front view and Back view of the fabricated prototype

The calibration and measurement process of the reflection coefficient of the proposed CSSRR antenna using the E5063A model of a vector network analyzer (VNA), operating within the frequency range of 100 kHz to 15 GHz is shown in Fig. 7.

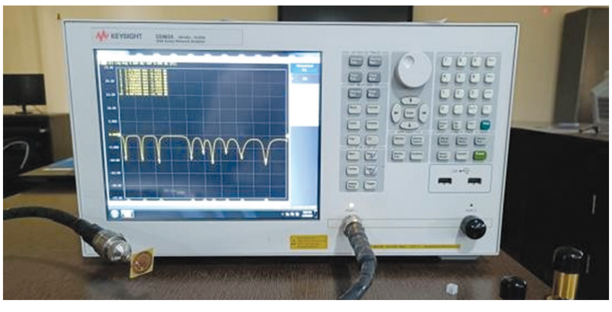

Fig. 7. Measuring the S-parameters using E5063A model of VNA and ranging 100KHz to 15 GHz

The reflection coefficient of the antenna has been verified with the simulated and measured results compared in Fig. 8. The operating bands are identified as 1.20, 2.10, 2.96, 4.70, 5.46, 5.98, 6.68, and 7.30 GHz. The reflection coefficient is below - 10 dB, indicating good performance, with only 10% of the power reflected and 90% radiated by the antenna.

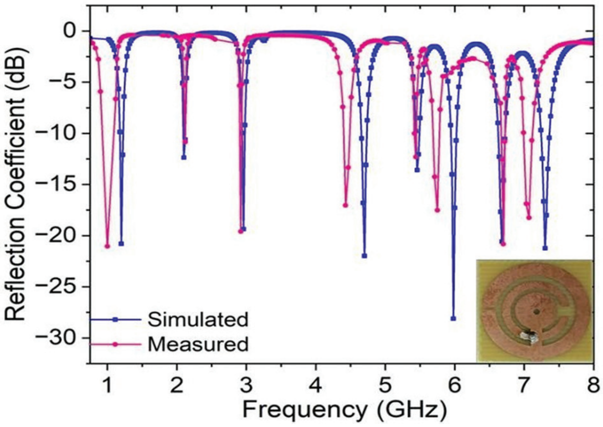

Fig. 8. Simulated and measured results of the proposed antenna design

The impedance bandwidth for each resonance of the antenna is shown in Table 2.

Table 2. Impedance Matching and Return loss Results

Resonance Frequency (*fr*) in GHz	Impedance Bandwidth (*IBW*) in GHz	Reflection Coefficient (S_{11}) in dB
1.22	1.1-1.25	-22
2.12	2.1-2.2	-13
3	2.9-3.2	-21
4.76	4.55-4.8	-23
5.4	5.3-5.45	-14
5.94	5.8-6.25	-28
6.70	6.6-6.78	-23
7.74	7.3-7.6	-24

The simulated and measured VSWR (Voltage Standing Wave Ratio) values are shown in Fig. 9. They are both below 2 and within the acceptable range for real-time applications in the relevant operating bands. At certain resonant frequencies, the VSWR is observed to be less than 1.5. The simulated and measured results were are in close agreement with each other.

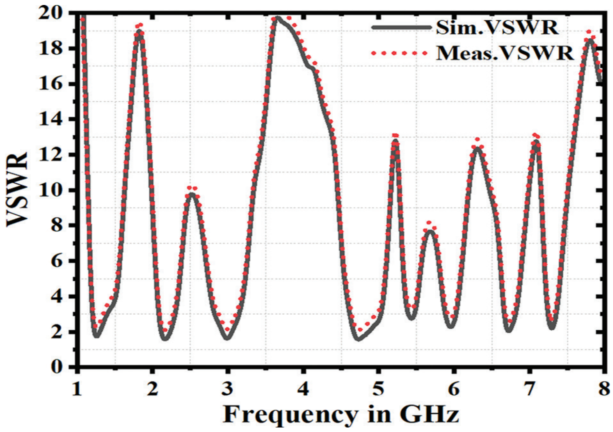

Fig. 9. Simulated and measured VSWR

Among the operational frequencies, the far-field patterns are measured for the frequencies where maximum impedance matching is achieved. Fig. 10 (a) illustrates the anechoic chamber setup from the inside, while Fig. 10 (b) shows the exterior setup used for measuring the radiation pattern and gain of the proposed antenna.

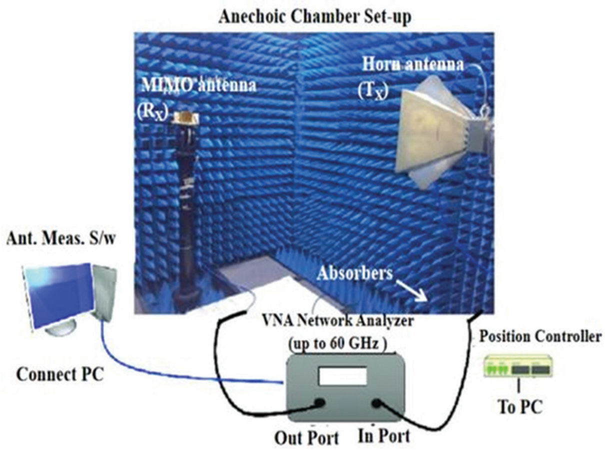

(a)

(b)

Fig. 10. Radiation and gain measuring setup in anechoic Chamber: (a) inside Setup (b) outside setup

The 2D radiation patterns of the E-plane ($\phi = 0^0$) and H-plane (($\phi = 90^0$) corresponding to the resonating frequencies at (a) 1.22 GHz, (b) 2.12 GHz, (c) 3.0 GHz, (d) 4.76 GHz, (e) 5.40 GHz, (f) 5.94 GHz, (g) 6.70 GHz, and

(h) 7.44 GHz, as shown in Fig. 11. The figure illustrates both the simulated and measured radiation patterns for these frequencies. The patterns demonstrate stable behavior, ensuring minimal cross-polarization and focused radiation in specific directions.

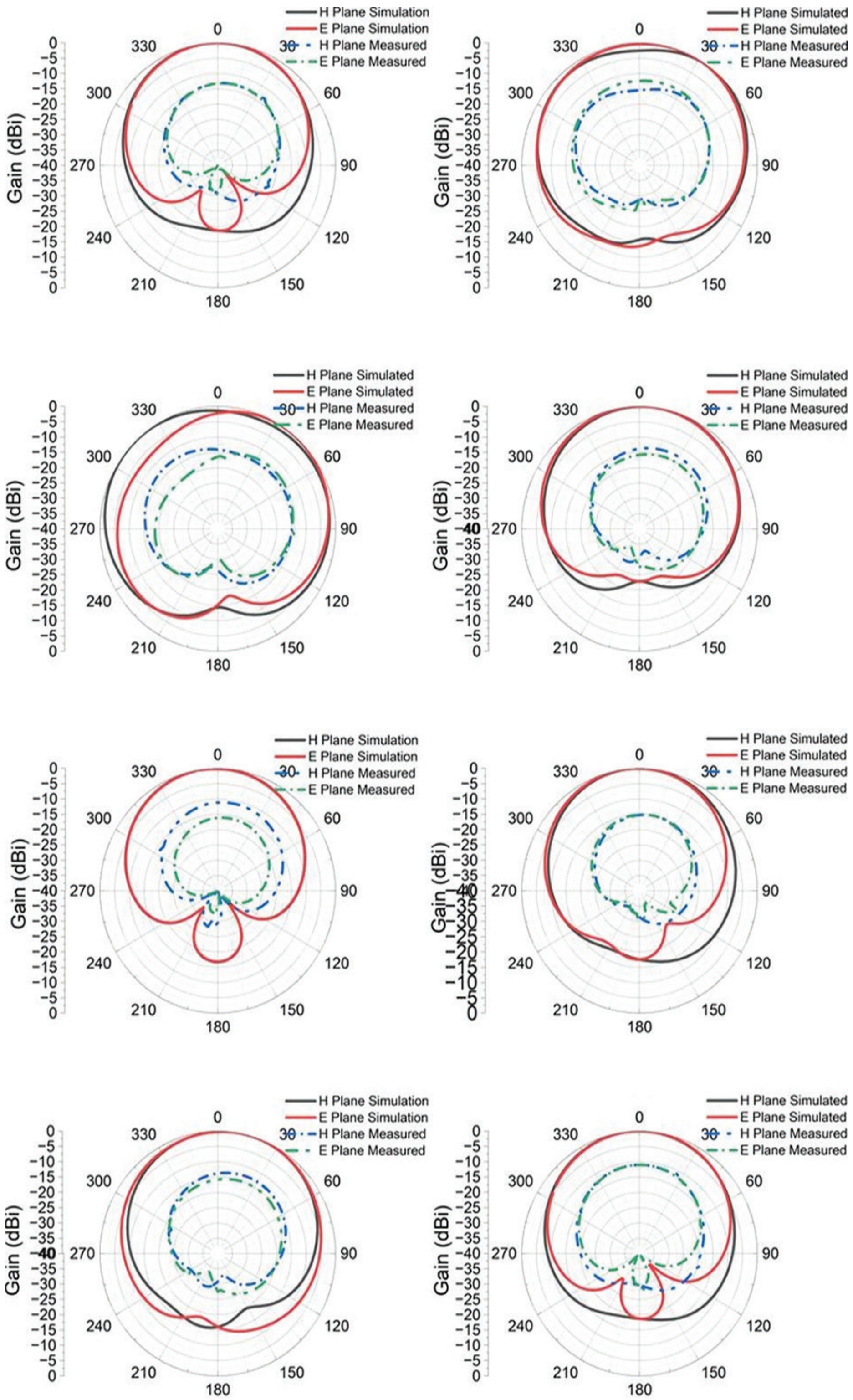

Fig. 11. Radiation pattern for (a) 1.2 GHz (b) 2.1 GHz (c) 2.9 GHz (d) 4.7 GHz (e) 5.4 GHz (f) 5.9 GHz (g) 6.6 GHz and (h) 7.3 GHz

Fig. 12. presents the simulated and measured peak gain and radiation efficiency of the proposed antenna design. The results demonstrate improved performance, with variations observed across different operating bands. The radiation efficiency ranges from 77% to 85% for the octa-band configuration of the proposed antenna. Table 3 provides the far-field simulated and measured results.

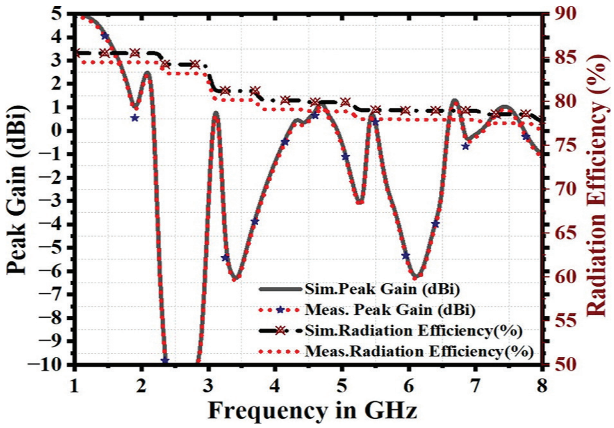

Fig. 12. Simulated and measured Peak Gain along with the Radiation Efficiency results of proposed design

Table 3. Simulated and measured peak gain and radiation efficiency at the corresponding resonant frequencies

f_r in GHz	Gain (dBi) (Sim.)	Gain (dBi) (meas)	Eff (Sim)	Eff (Meas)
1.22	4.80	4.71	85.10	84.27
2.12	2.81	2.68	85.44	84.46
3.0	0.98	0.86	81.2	80.17
4.76	1.39	1.16	79.9	78.87
5.40	1.167	1.041	79.2	77.99
5.94	0.50	0.377	79	77.99
6.70	0.30	0.17	78.5	77.92
7.44	1.04	0.92	78.5	77.52

A comprehensive analysis of the proposed antenna design compared to state-of-the-art models demonstrates its significant advancements in key performance areas. The proposed design excels in achieving enhanced multiband operation, better impedance matching, and improved integration potential with modern wireless systems, all while maintaining a compact and low-profile structure out of all the existing antennas. The findings of this research are summarized in Table 4 and they illustrate the innovative contributions of the design and it can be observed that the challenges such as achieving simultaneous miniaturization, multi- band operation and stable gain are resolved by this proposed antenna. This study highlights the effectiveness and practicality of the antenna, marking it as a valuable solution for advanced wireless communication applications.

5. CONCLUSION

The proposed antenna design effectively achieves octa- band frequency response through a compact radiator based on a circular-shaped split ring resonator (CSSRR) structure. Operating at 1.22, 2.12, 3, 4.76, 5.4, 5.94, 6.70, and 7.44 GHz, the antenna exhibits excellent radiation characteristics, with a peak gain of 4.71 dBi and radiation efficiency ranging from 74% to 85% across all bands. Its compact size, cost-effectiveness, and superior performance make it an ideal solution for sub-6 GHz 5G applications and other wireless communication systems, including Wi-Fi, WLAN, and WiMAX. Furthermore, it has the potential to support higher frequency bands, while maintaining optimized efficiency and gain. This makes the antenna suitable for emerging use cases in autonomous vehicles, smart cities, and defense systems. Overall, the proposed antenna provides a strong platform to address the evolving needs of modern and next-generation wireless communication systems.

Table 4. Comparative study between the state-of-the-art work of the proposed design

Ref.	Area ($\lambda 0 \times \lambda 0$)	No. of Bands	Freq. Ratio	Freq. band (fH – fL)	Gain (dBi)	Eff(%)
7	1.16 × 1.16	6	2.01	11.2	1.34	90
9	0.28 × 0.24	6	2.84	3.87	2.81	92
10	0.29 × 0.29	6	2.05	2.63	-	-
11	0.35 × 0.14	6	2.53	3.63	7.39	-
12	0.55 × 0.55	6	5.58	23.46	2.3	71
13	0.57 × 0.57	6	7.51	22.55	3.23	87
14	0.27 × 0.27	7	4.25	5.6	-	-
15	1.17 × 1.17	7	2.91	53.9	7.16	99
29	0.26 × 0.178	8	7.25	4.5	4	-
TW	0.08 × 0.08	8	6.08	6.1	4.71	85

6. REFERNCES

[1] R. Saleem, M. Bilal, H. T. Chattha, A. Mushtaq, M. F. Shafique, "An FSS based multiband MIMO system incorporating 3D antennas for WLAN/ WiMAX/5G cellular and 5G Wi-Fi applications", IEEE Access, Vol. 7, 2019, pp. 144732-144740.

[2] Y. Liu, L. Shafai, D. Isleifson, C. Shafai, "Split Ring Antennas and Their Application for Antenna Miniaturization", Sensors, Vol. 23, No. 2, 2023, p. 846.

[3] R. A. Mellita, S. S. Karthikeyan, P. Damodharan, D. S. Chandu, "A miniaturized quad-band frequency selective surface for C-band applications", Journal of Electromagnetic Waves and Applications, Vol. 35, No. 14, 2021.

[4] R. K. Saraswat, M. Kumar, "Implementation of an Octa-band Metamaterial Inspired Frequency Band Reconfigurable Antenna for IoT applications in Wireless Standards", IETE Journal of Research, Vol. 70, No. 5, 2022.

[5] S. E. Kilani, L. E. Abdellaoui, J. Zbitou, M. Latrach, "A compact dual band PIFA antenna for GPS and ISM BAND applications", Indonesian Journal of Electrical Engineering and Computer Science, Vol. 14, No. 3, 2019, pp. 1266-1271.

[6] M. Thirupathi, B. Harikrishna, "Reduced mutual coupling multiband MIMO patch antenna with swastik type mushroom EBG", Indonesian Journal of Electrical Engineering and Computer Science, Vol. 14, No. 1, 2019, pp. 490-494.

[7] A. Sabah, M. J. Frhan, "A new patch antenna for ultra wide band communication applications", Indonesian Journal of Electrical Engineering and Computer Science, Vol. 18, No. 2, 2020, pp. 848-855.

[8] S. Liu, Z. Wang, Y. Dong, "Compact wideband SRR-inspired antennas for 5G microcell applications", IEEE Transactions on Antennas and Propagation, Vol. 69, No. 9, 2021, pp. 5998-6003.

[9] V. Rajeshkumar, R. Rajkumar, "SRR loaded compact tri-band MIMO antenna for WLAN/WiMAX applications", Progress in Electromagnetics Research Letters, Vol. 95, 2021, pp. 43-53.

[10] A. El Yousfi, A. Lamkaddem, K. A. Abdalmalak, D. Segovia-Vargas, "A miniaturized triple-band and dual-polarized monopole antenna based on a CSRR perturbed ground plane", IEEE Access, Vol. 9, 2021, pp. 164292-164299.

[11] S. P. J. Christydass, N. Gunavathi, "Dual-band complementary split-ring resonator engraved rectangular monopole for GSM and WLAN/ WiMAX /5G sub-6 GHz band (new radio band)", Progress In Electromagnetics Research C, Vol. 113, 2021, pp. 251-263.

[12] S. Ullah, S. Ahmad, J. A. Flint, "A multi-band switchable antenna for Wi-Fi, 3G advanced, WiMAX, and WLAN wireless applications", International Journal of Microwave and Wireless Technologies, Vol. 10, No. 8, 2018, pp. 991-997.

[13] P. Chaurasia, B. Kanaujia, S. Dwari, M. K. Khandelwal, "Antenna with hexa-band capabilities for multiple wireless applications", Progress In Electromagnetics Research C, Vol. 82, 2018, pp. 109-122.

[14] V. Singh, B. Mishra, A. K. Dwivedi, R. Singh, "Inverted l-notch loaded hexa band circular patch antenna for x, ku/k band applications", Microwave and Optical Technology Letters, Vol. 60, No. 8, 2018, pp. 2081-2088.

[15] J. O. Abolade, D. B. Konditi, V. M. Dharmadhikary, "Compact hexa-band bio-inspired antenna using asymmetric microstrip feeding technique for wireless applications", Heliyon, Vol. 7, No. 2, 2021.

[16] R. Dhara, T. Kundu, M. Sanoj, "Circularly polarized hexa-band planar slot antenna for WLAN and wireless communication application", Radioelectronics and Communications Systems, Vol. 65, No. 1, 2022, pp. 48-59.

[17] D. Tiwari, J. A. Ansari, A. K. Saroj, M. Kumar, "Analysis of a miniaturized hexagonal sierpinski gasket fractal microstrip antenna for modern wireless communications", AEU-International Journal of Electronics and Communications, Vol. 123, 2020, p. 153288.

[18] R. Sachan, D. C. Dhubkarya, "Photonic bandgap hepta-band stacked microstrip antenna for l, S and C band applications", Wireless Personal Communications, Vol. 116, No. 3, 2021, pp. 1913-1931.

[19] W. Shahjehan, I. Hussain, I. Ali, A. Riaz, P. Uthansakul, "Hepta-band antenna for 5G applications", Wireless Personal Communications, Vol. 125, No. 3, 2022, pp. 2031-2054.

[20] D. Huang, Y. Wang, "Eight-band antenna for full-screen metal frame LTE mobile phones", IEEE Trans. Antennas Propagation, Vol. 67, No. 3, 2018, pp. 1527-1534.

[21] Y. Wang, Z. Du, "Wideband monopole antenna with less nonground portion for octa-band WWAN/LTE mobile phones", IEEE Transactions on Antennas and Propagation, Vol. 64, No. 1, 2015, pp. 383-388.

[22] D. Huang, Y. Wang, "An octa-band monopole antenna with a small nonground portion height for LTE/WWAN mobile phones", IEEE Transactions on Antennas and Propagation, Vol. 65, No. 2, 2016, pp. 878-882.

[23] K.-L. Wong, P.-R. Wu, "Dual-wideband linear open slot antenna with two open ends for the LTE/WWAN smartphone", Microwave and Optical Technology Letters, Vol. 57, No. 6, 2015, pp. 1269-1274.

[24] D. Huang, Z. Du, "Eight-band antenna with a small ground clearance for LTE metal-frame mobile phone applications", IEEE Antennas and Wireless Propagation Letters, Vol. 17, No. 1, 2017, pp. 34-37.

[25] R. Tang, Z. Du, "Wideband monopole without lumped elements octa-band narrow-frame LTE smartphone", IEEE Antennas and Wireless Propagation Letters, Vol. 16, 2016, pp. 720-723.

[26] D. Huang, Z. Du, Y. Wang, "Compact octa-band monopole antenna with independently tuning for WWAN/LTE mobile phones", Microwave and Optical Technology Letters, Vol. 59, No. 1, 2017, pp. 208-214.

[27] K.-L. Wong, C.-Y. Tsai, "Half-loop frame antenna for the LTE metal casing tablet device", IEEE Transactions on Antennas and Propagation, Vol. 65, No. 1, 2016, pp. 71-81.

[28] Z.-Q. Xu, Q.-Q. Zhou, Y.-L. Ban, S. S. Ang, "Hepta-band coupled fed loop antenna for LTE/WWAN unbroken metal-rimmed smartphone applications", IEEE Antennas and Wireless Propagation Letters, Vol. 17, No. 2, 2017, pp. 311-314.

[29] Y. Liu, W. Cui, Y. Jia, A. Ren, "Hepta-band metal-frame antenna for LTE/WWAN full-screen smartphone", IEEE Antennas and Wireless Propagation Letters, Vol. 19, No. 7, 2020, pp. 1241-1245.

[30] D. Wu, S. Cheung, T. Yuk, "A compact and low- profile loop antenna with multiband operation for ultra-thin smart phones", IEEE Transactions on Antennas and Propagation, Vol. 63, No. 6, 2015, pp. 2745-2750.

[31] Ab Rashid, A. Hafizun, B. H. Ahmad, M. Z. A. Abd Aziz, "CPW Fractal Antenna with Third Iteration of Pentagonal Sierpinski Gasket Island for 3.5 GHz WiMAX and 5.2 GHz WLAN Applications", International Journal of Electrical and Computer Engineering Systems, Vol. 14, No. 2, 2023, pp. 129-134.

[32] M. Abbasi, T. A. Latef, "Wideband circularly polarized fractal antenna with SSRR metasurface for 5G applications", International Journal of Electrical and Computer Engineering Systems, Vol. 15, No.1, 2024, pp. 89-98.

[33] K. Vinayagam, R. Natarajan, "Polarization Reconfigurable Patch Antenna Using Parasitic Elements for Sub-6 GHz Applications", International Journal of Electrical and Computer Engineering Systems, Vol. 16, No. 1, 2025, pp. 1-7.

[34] F. Liu, J. Guo, Z. Zhao, L. Zhao, G.-L. Huang, Y. Li, Y. Yin, "Coupled meander-line resonators for mutual coupling suppression of microstrip patch antennas", International Journal of RF and Microwave Computer-Aided Engineering, Vol. 31, No. 3, 2021, p. e22528.